CrossMark

ORIGINAL ARTICLE

Utilization of coal bottom ash to improve thermal insulation of construction material

Pincha Torkittikul[1] · Thanongsak Nochaiya[2] · Watcharapong Wongkeo[3] · Arnon Chaipanich[4]

Abstract Concerns with sustainable solid waste management and recycling have become increasingly prominent in all sectors of the economy. In light of this, this research investigates the possibility of utilizing coal bottom ash (waste from thermal power plants) as a substitute for fine aggregate in mortar and concrete. The chemical composition, microstructure and mechanical properties, including workability, density, water absorption, compressive strength and thermal conductivity, of mortar and concrete incorporating coal bottom ash in partial and full replacement of sand were investigated, and the results were compared to the data for conventional mortar and concrete. The results show that the density of mortar and concrete was noticeably decreased with increasing coal bottom ash content. In addition, despite the permeable pore space of mortars and concretes increasing with increasing levels of coal bottom ash, the use of coal bottom ash does not significantly affect the compressive strength of concrete. Furthermore, the mortars and concretes containing coal bottom ash exhibited good thermal insulation properties; thermal conductivity values decreased significantly with increasing coal bottom ash content, and the thermal conductivity of mortar and concrete with 100 % coal bottom ash showed a decrease of 68.61 and 46.91 %, respectively, as compared to that of the control.

Introduction

Worldwide, the creation of waste products continues to increase due to continued demand for resources used by humans, and this is considered one of the most pressing environmental problems which we face. It has therefore become necessary to manage and recycle industrial, residential and other wastes as well as to use non-renewable resources wisely and efficiently. Since, because of its valuable properties, concrete is widely used in construction, an extensive body of research on waste recycling in concrete has been developed and the results disseminated to decision makers [1–5]. Some types of waste can be incorporated into concrete, either as part of the cement mixture or as aggregate. This helps increase the sustainability of the construction materials [4, 5]. Some wastes or by-products from industry have been successfully utilized in this manner, and this includes fly ash used as a constituent in cement to produce Portland fly ash cement [6–10]. In addition, wastes or by-products larger than cement particles may be used as aggregates in mortar or concrete. This includes waste ceramic [11, 12], recycled plastic [13, 14], recycled glass [15, 16] and waste polyethylene terephthalate bottles [17].

After combustion of coal within the furnace of a coal-fired thermal power plant, the finer particles of non-

✉ Pincha Torkittikul
  pincha_t@lpru.ac.th

[1] Department of Civil Technology, Faculty of Industrial Technology, Lampang Rajabhat University, Lampang 52100, Thailand

[2] Department of Physics, Faculty of Science, Naresuan University, Phitsanulok 65000, Thailand

[3] Physics and General Science Program, Faculty of Science and Technology, Nakhon Ratchasima Rajabhat University, Nakhon Ratchasima 30000, Thailand

[4] Construction Materials Research Unit, Faculty of Science, Chiang Mai University, Chiang Mai 50200, Thailand

combustible ash are extracted in electrostatic precipitators. Some melted ash accumulates on the boiler walls and solidifies to form mass particles, which falls to the bottom of furnace and is cooled in water. The coal ash collected from the electrostatic precipitators and from the bottom of the furnace is called fly ash and coal bottom ash, respectively [18]. In recent years, the utilization of fly ash in mortar and concrete has received considerable attention due to its potential application in civil engineering for reasons including its reduced heating during hydration, its low permeability and its resistance to sulphate attack [19, 20]. However, there have only been limited studies on the use of coal bottom ash as a partial replacement of Portland cement [21] or as a partial replacement of fine aggregate [22–25]. Andrade et al. [22] reported that the use of coal bottom ash at levels of up to 10 % as a replacement material for Portland cement could improve the mechanical properties of concrete. Lee et al. [23] investigated the feasibility of utilizing coal bottom ash as an aggregate in fibre-reinforced cellular concrete and suggested that coal bottom ash could be applied as a construction material but warned that it may not improve the compressive strength of fibre-reinforced cellular concrete. Yüksel et al. [24] found that using a combination of coal bottom ash and granulated blast furnace slag as a fine aggregate in concrete would result in improved durability of concrete but the compressive strength was found to decrease by 31.8 % since bottom ash was used as a fine aggregate replacement at 50 % by volume. Hussain et al. [25] discussed that the use of bottom ash as partial substitution of fine aggregate reduced the curing sensitivity of concrete especially at a lower mass ratio of water to binder due to its internal curing effect. Although the replacement of sand with bottom ash seems to result in the reduction of compressive strength due to an increase in the volume of all pores in mortars and concretes [26–28], previous research demonstrated that the presence of pores influences the thermal conductivity of the materials [29, 30]. Kim et al. [29] investigated the thermal properties of lightweight aggregate concrete with a high volume of entrained air generated by an air-entraining agent introduced during the mixing process. The results showed that the thermal conductivity of concrete linearly decreased as the porosity increased. Wang et al. [30] tested the thermal conductivity of lightweight material produced from cement, sewage sludge ash and aluminium powder. The results indicated that the addition of sewage sludge ash increased the volume of pores smaller than 10 μm and thus the thermal conductivity of lightweight cement containing sewage sludge ash (0.185 W/m K) was lower than the control cement (0.571 W/m K) which was due to the porous characteristics of the material.

Unfortunately, studies on thermal insulation and the microstructure of mortar and concrete containing coal bottom ash have been very limited. This study therefore aims to investigate the microstructure and mechanical properties of mortar and concrete containing various amounts of coal bottom ash. The properties which are investigated include workability, compressive strength, density, permeable pore space, water absorption, microstructure and thermal conductivity. This study may help reduce the use of non-renewable material resources and therefore contribute to increased sustainability.

Materials and methods

Materials

The cement used in this study was ordinary Portland cement type I (OPC) conforming to ASTM C150 [31] and it had a specific gravity of 3.15. The analysis of the chemical composition carried out by X-ray fluorescence techniques is presented in Table 1.

Crushed gravel with a maximum size of 19 mm, according to ASTM C33 [32], was used as a coarse aggregate. The grain size distribution of the crushed gravel is shown in Fig. 1. Both the water absorption and the specific gravity of crushed limestone were measured according to ASTM C127 [33]. These were approximately 1.0 % by mass and 2.71, respectively (Table 2).

Well-graded natural sand with a size less than 4.75 mm was used in all mortar mixtures. The grain size distribution of the sand is shown in Fig. 1. The fineness modulus of sand was 2.95 obtained by the summation of the cumulative percent retained on the standard sieve (Fig. 1). The water absorption and specific gravity of sand, measured according to ASTM C128 [34], were approximately 1.12 % by mass and 2.60, respectively (Table 2). The particle shapes and surface texture of the sand, observed by scanning electron microscope (SEM), are shown in Fig. 2. As can clearly be seen from the SEM images, the sand is slightly angular, with a smoother surface texture (Fig. 2c, e) than that of coal bottom ash (Fig. 2d, f). The analysis of the chemical composition, measured by X-ray fluorescence technique (XRF), is presented in Table 1.

The coal bottom ash (BA) used in this study was obtained from Mae Moh power plant, which is operated by the Electricity Generating Authority of Thailand. The dried coal bottom ash was sieved through a sieve mesh Nos. 4, 8, 16, 30, 50 and 100. The grain size distributions of both sand and coal bottom ash aggregates were kept the same in order to allow a direct comparison of their effects on compressive strength (Fig. 1). Optical photographs and SEM images of coal bottom ash aggregate are shown in Fig. 2. Water absorption and the specific gravity of coal bottom ash aggregate were measured according to ASTM

Table 1 Chemical composition of Portland cement, sand and coal bottom ash

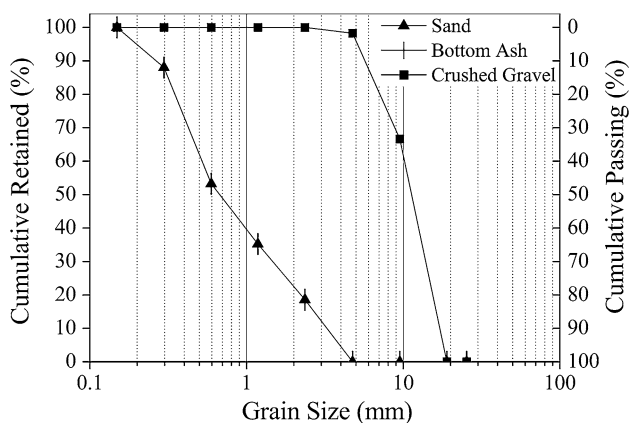| Oxide	Portland cement (wt%)	Sand (wt%)	Coal bottom ash (wt%)
SiO_2	20.18	95.19	36.84
Al_2O_3	4.98	3.05	18.28
CaO	63.74	–	18.43
Fe_2O_3	3.44	0.57	15.46
MgO	2.66	–	2.62
K_2O	0.64	–	2.29
P_2O_5	–	–	0.17
Na_2O	0.45	–	0.75
TiO_2	–	–	0.90
MnO_2	–	–	0.20
SO_3	2.46	–	0.74
Loss on ignition (LOI)	1.45	1.19	2.02

Fig. 1 Grain size distribution of fine and coarse aggregates

C128 [34], and these were found to be 15 % by mass and 1.75, respectively. Particle shapes and the surface texture of coal bottom ash were checked by optical microscope (OM) and SEM and are shown in Fig. 2d, f respectively. As can be seen, coal bottom ash particles are angular and rougher than sand. The chemical analysis carried out by XRF is presented in Table 1.

Mix proportions

The details of the mix proportions identified by specific codes are given in Table 3. The characters 'M' and 'C' represent mortar and concrete, respectively. The number next to the characters, for example '0', '10', etc., refers to the proportion of fine aggregate replaced by coal bottom ash. The amount of Portland cement, sand, coal bottom ash, coarse aggregate and water shown in Table 3 was back-calculated based on total volume of mixture and density values of the raw materials. Coal bottom ash was used as sand replacement at 10, 20, 30, 50, 70, 80 and 100 % by volume in mortar mixtures. For concrete mixtures, coal bottom ash was used as sand replacement at 20, 50, 80 and 100 % by volume.

Workability

The workability of the mortar was measured according to ASTM C1437 [35]. The makeup of each mortar mix (blended in a mechanical mixer) is shown in Table 3. After mixing, the fresh mortar was added to a flow-table mould in two approximately equal layers, with each layer compacted by 25 strokes of a tamper. The excess mortar was skimmed off with a palette knife, the mould was slowly raised vertically and then the table was jolted for 15 s at a constant tempo. Measurement of the workability was obtained by the average of four values of the diameter of the fresh mortar measured in two directions at right angles to one another.

The workability of concrete was investigated according to ASTM C143 [36]. After each fresh concrete mix was prepared (as per the details in Table 3), the fresh concrete was filled in a slump mould placed on a flat surface and then tamped with a steel rod 25 times at three different layers. After the top layer was tamped, the surface of the fresh concrete was struck off by means of a screening and rolling motion with a tamping rod. The mould was

Table 2 Physical properties of aggregates

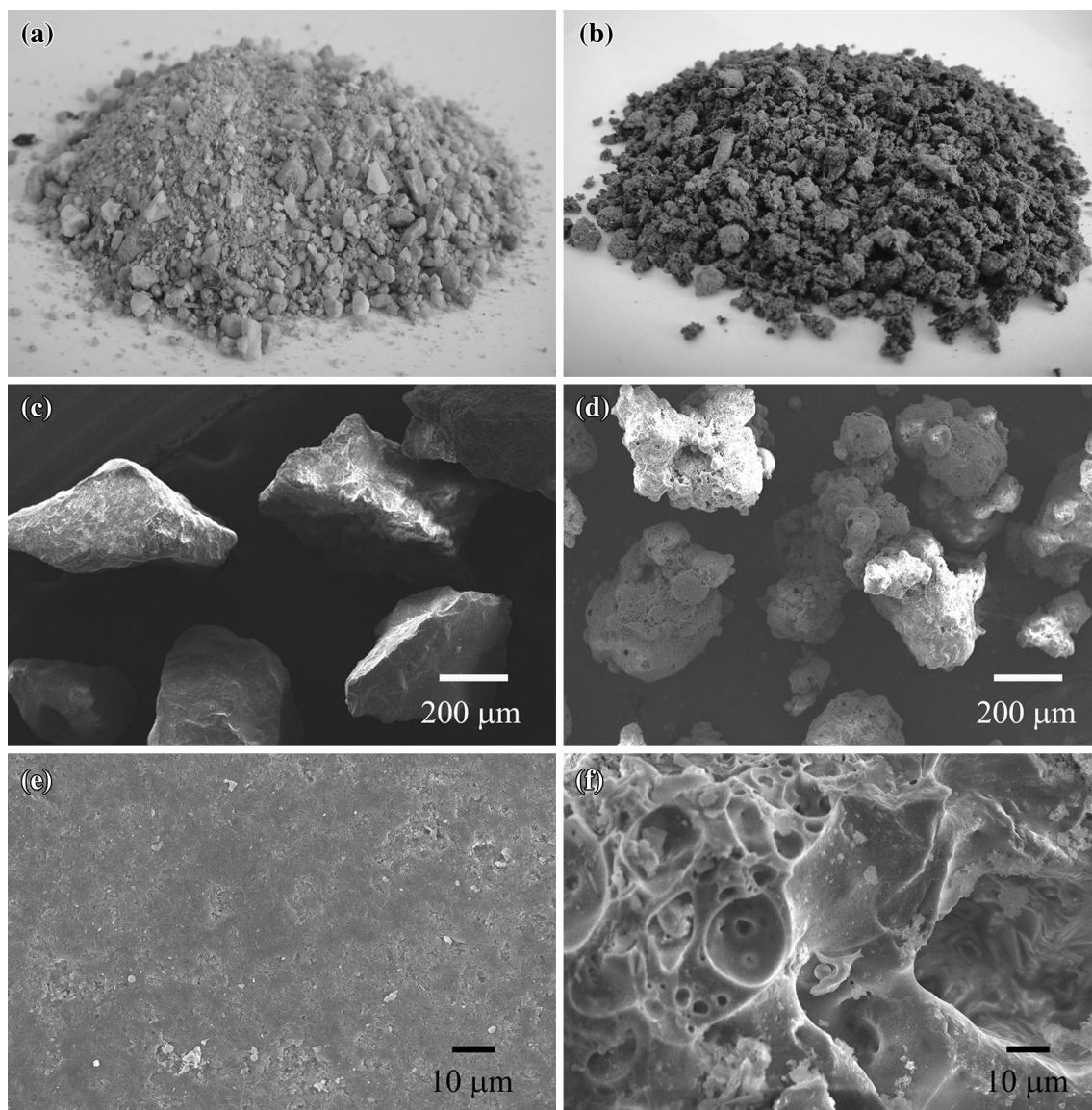| Aggregates	Maximum size (mm)	Specific gravity (−)	Water absorption (%)	Fineness modulus (−)
Sand	4	2.60	1.12	2.95
Coal bottom ash	4	1.75	15.48	2.95
Crushed gravel	20	2.71	1.03	6.65

Fig. 2 **a** Illustration of natural sand, **b** illustration of coal bottom ash, **c** SEM of sand particles, **d** SEM of coal bottom ash particles, **e** SEM of natural sand surface and **f** SEM of coal bottom ash surface

immediately removed from the fresh concrete by raising it carefully in a vertical direction. The slump was immediately measured by determining the vertical difference between the top of the mould and the displaced original centre of the top surface of the specimen.

Water absorption, apparent density and volume of permeable pore space

The tested specimens were prepared according to the procedure outlined in the previous section and in accordance with ASTM C305 [37]. After 28 days of curing in water, the specimens were removed from the water, dried in an oven at a temperature of 110 ± 5 °C for 72 h and then cooled in a desiccator to room temperature. The mass of the dry specimen was determined and recorded as A. The dried specimens were then immersed in tap water at a temperature of approximately 21 °C for 72 h. The specimens were boiled, covered with tap water for 5 more hours, allowed to cool by natural heat loss for 24 h and then surface-dried by removing surface moisture with a towel. The mass was recorded as B. Finally, the boiled specimen was weighed in water and this mass was designated as C. The values of A, B and C were used to determine water absorption, apparent density and volume of permeable pores (void) of the specimen using a calculation as follows, where ρ_w is the density of water [38]: the reported results are from the average of three specimens.

Table 3 Mix proportion of mortars and concretes containing various amounts of coal bottom ash

Part	Mix designation	Coal bottom ash (%)	Cement (kg/m^3)	Sand (kg/m^3)	Coal bottom ash (kg/m^3)	Gravel (kg/m^3)	Water (kg/m^3)
Mortar	M0BA	0	562	1405	0	–	296
	M10BA	10	562	1264	94	–	309
	M20BA	20	562	1124	189	–	321
	M30BA	30	562	983	283	–	334
	M50BA	50	562	702	472	–	359
	M70BA	70	562	421	661	–	385
	M80BA	80	562	281	756	–	397
	M100BA	100	562	–	945	–	422
Concrete	C0BA	0	375	562	–	1252	229
	C20BA	20	375	449	75	1252	239
	C50BA	50	375	281	189	1252	254
	C80BA	80	375	112	302	1252	269
	C100BA	100	375	–	378	1252	279

$$\text{Water absorption} = \left(\frac{B - A}{A}\right) \times 100 \qquad (1)$$

$$\text{Apparent density} = \left(\frac{B}{BC}\right) \times \rho_w \qquad (2)$$

$$\text{Permeable pore space} = \left(\frac{BA}{BC}\right) \times 100. \qquad (3)$$

Thermal conductivity

The constituents of specimens were mixed together according to ASTM C305 and prepared in cylinder-shaped moulds (25 mm in diameter and 100 mm in height for mortar, 100 mm in diameter and 100 mm in height for concrete) [37]. After 28 days of curing in water, the specimens were removed from water and dried in an oven at a temperature of 110 ± 5 °C for 72 h and then cooled in a desiccator to room temperature. Thermal conductivity tests were carried out using KD2 Pro Thermal Properties Analyser. This complied with ASTM D5334 [39]. The reported results are from the average of four specimens.

Compressive strength

All mortar constituents were weighed according to the mix proportions shown in Table 3 and then mixed together following the mixing procedures in ASTM C305 [37]. After setting for 24 h, the specimens were removed from the moulds and cured in pH 12 water at room temperature. The compressive strength of the mortars was tested at 3, 7, 14, 28, 60 and 120 days using ELE International ARD1500 standards. The reported results are the averages of three samples.

All concrete constituents were weighed according to the mix proportions shown in Table 3 and mixed together following the procedures detailed in ASTM C192 [40]. The fresh concrete was cast and compacted in 150-mm cubic moulds, smoothed and covered with plastic film to prevent moisture loss during curing in the moulds. After setting for 24 h, the specimens were removed from the moulds and cured in pH 12 water at room temperature. The compressive strength of the concretes was measured at 7, 28 and 160 days using ELE International ARD1500 standards. The reported results are the averages of three samples.

Scanning electron microscopy (SEM)

Raw materials and fragments of mortar specimens resulting from tests for compressive strength were tested for morphology and chemical characteristics. Small pieces of mortar containing various amounts of coal bottom ash were attached to double-sided carbon tape mounted on a brass stub. All samples were coated with gold operated by 10–20 mA DC current. The elemental composition and morphology of the samples were determined at the Electron Microscopy Research and Service Center (EMRSC) of Chiang Mai University using low vacuum SEM with a JEOL JEM-5910LV microscope linked to an energy-dispersive X-ray spectrometry (EDS) unit.

X-ray diffraction (XRD)

The crystalline phases of natural sand and coal bottom ash were investigated using XRD technique (Philips X'Pert-MRD, The Netherlands). Both fine aggregates were ground and sieved through a sieve mesh No. 100 (opening 150 μm). The powder was weighed and approximately 5 g was used to determine the crystalline phases, and the measurements were made with a 2θ step interval of 5°–80°.

Results and discussion

Workability

The effect of using coal bottom ash as a replacement for fine aggregates on the workability of mortars and concretes is presented in Fig. 3. The workability of mortars was assessed based on the measured flow of the fresh mortar. The results show that the flow of mortars slightly decreased with increasing coal bottom ash content. The flow of the 100 % coal bottom ash mortar was approximately 16.1 cm, which was a 34.3 % decrease compared to the control mortar.

Considering the workability of the concrete, as can be seen from the results of the tests, the slump was clearly reduced by increasing the proportion of coal bottom ash. Nonetheless, there was no detrimental effect on slump values when the coal bottom ash was added at 20 % by volume. In this case, the slump values were similar to the control concrete. However, when coal bottom ash was used as sand replacement at 80 and 100 % by volume, the slump values dropped close to 0 (4 and 1 cm, respectively). The decrease in workability of mortars and concretes can be attributed to the angular shape and rough surface of coal bottom ash which might lead to an increase in friction between the mixing components [28].

Density

The effect of coal bottom ash on the density of mortars and concretes at 28 days is shown in Fig. 4. As can be seen, the wet bulk density of mortars and concrete containing coal bottom ash was lower than that of the control group, and it was also inversely proportional to the amount of coal bottom ash. When sand was entirely replaced with coal bottom ash, the density of mortar at the age of 28 days was 1.83 g/cm³ and that of the concrete at the same age was 2.21 g/cm³. This represents a decrease of 12.86 and 6.36 % compared to that of the control mortar and concrete, respectively. The cause of the decrease in density can be explained by two factors. First, this may occur due to the physical characteristics of coal bottom ash since the specific gravity of coal bottom ash is lower than that of the sand and this results in a reduction in density of the mortars and concretes. The second reason is that mortars and concretes containing coal bottom ash require more water and the presence of excess water forms internal voids in hardened mortars and concretes [41, 42]. In addition, the reduction in the density of both mortar and concrete with respect to the amount of coal bottom ash appears to be linear with a correlation factor (R^2 value) close to 1.

Permeable pore space and water absorption

The permeable pore space and water absorption of mortars and concretes are presented in Table 4. The results indicate that theses increased with the increase in the levels of sand being replaced by coal bottom ash [28]. The permeable pore space of mortars and concrete increased from 21.91 to 37.05 % and 15.48 to 21.31 %, respectively, with the use of 100 % coal bottom ash as compared to that of the control mix. For the water absorption values of the specimens, mortars and concretes containing coal bottom ash at 100 % by volume exhibited the highest values, which were 25.21 and 10.78 %, respectively. These represented an increase of 56.01 and 34.79 % respectively, as compared to the control mix.
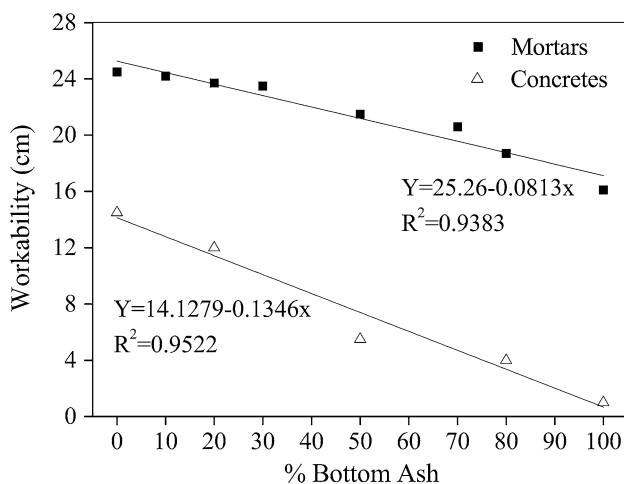

Fig. 3 Relationship between workability and amount of coal bottom ash
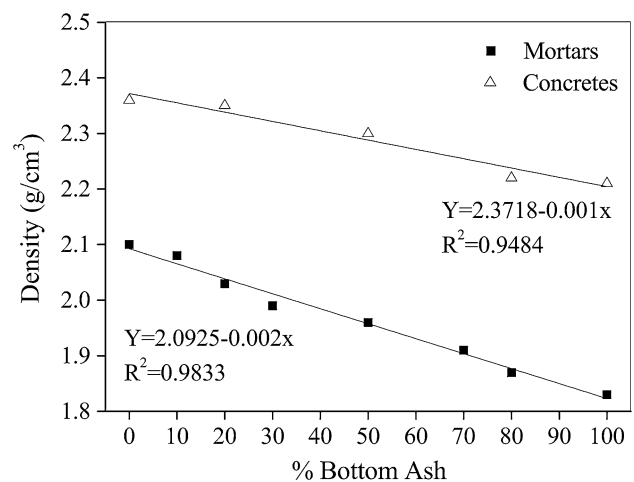
$$Y = 25.26 - 0.0813x$$
$$R^2 = 0.9383$$

$$Y = 14.1279 - 0.1346x$$
$$R^2 = 0.9522$$

Fig. 4 Relationship between density and amount of coal bottom ash

$$Y = 2.3718 - 0.001x$$
$$R^2 = 0.9484$$

$$Y = 2.0925 - 0.002x$$
$$R^2 = 0.9833$$

Table 4 Summary of the permeable pore space and water absorption of mortars and concretes

Mix	Permeable pore space (%)	Water absorption (%)
M0BA	21.91	11.09
M10BA	23.27	12.86
M20BA	25.00	13.02
M30BA	26.35	14.34
M50BA	29.22	16.15
M70BA	32.12	19.81
M80BA	34.16	22.98
M100BA	37.05	25.21
C0BA	15.48	7.03
C20BA	15.72	7.16
C50BA	17.12	8.45
C80BA	20.63	10.25
C100BA	21.31	10.78

Fig. 5 Relationship between thermal conductivity and amount of coal bottom ash

Thermal conductivity

A similar trend of thermal conductivity of mortars and concretes is shown in Fig. 5. As can be seen, it is interesting to note that the mortars and concretes containing coal bottom ash exhibited good thermal insulation properties since thermal conductivity values show a significant decrease with increasing coal bottom ash content. More precisely, the thermal conductivity of mortar decreases from 1.666 to 0.523 W/m K and that of concrete decreases from 2.052 to 1.089 W/m K with the replacement of sand by coal bottom ash at 100 % by volume compared to that of the control mix. These can be expressed as 68.61 and 46.91 % reduction in thermal conductivity for mortar and concrete, respectively (Table 5). Thermal conductivity plotted as a function of the volume of the permeable voids is shown in Fig. 6. As can be seen, the thermal conductivity of mortar was found to decrease linearly as the porosity increased ($R^2 = 0.9854$). In addition, the cross section of specimen with and without bottom ash supported the thermal conductivity result since a lot of pores were found in the specimen with 100 % bottom ash (Fig. 7). This indicates that the presence of pores in the material is an important factor in thermal insulating performance [43, 44].

Compressive strength

The compressive strength and relative strength of mortars and concretes containing various proportions of coal bottom ash are presented in Tables 6 and 7, respectively. As can be seen, with increasing duration of the curing period, the strength of mortars containing coal bottom ash in partial or full replacement of fine aggregate showed
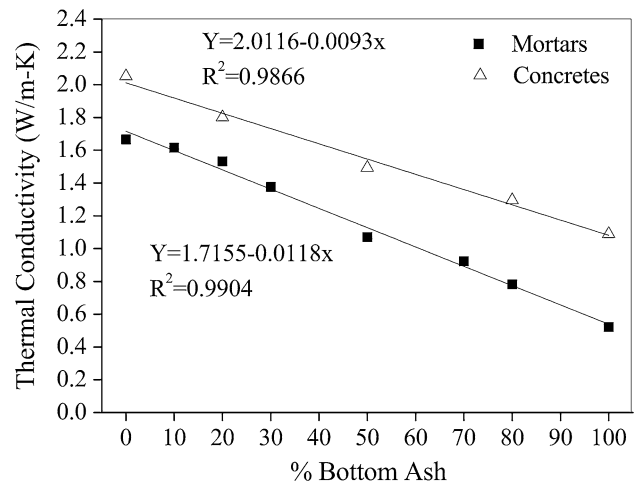
continuous and significant increases. Mortars with various levels of coal bottom ash developed compressive strengths ranging from 27.20 to 36.85 and 33.45 to 49.21 at 7 and 28 days, respectively. At these time points, concrete with various amounts of coal bottom ash developed compressive strengths ranging from 20.50 to 31.92 and 31.39 to 32.84, respectively. The relationship between the compressive strength and the proportion of coal bottom ash is shown in Fig. 8. The results indicate that the compressive strength of mortars and concretes is linearly correlated with the use of coal bottom ash, since these showed a correlation factor (R^2 value) of 0.9659 and 0.8182, respectively.

In addition, the difference in the compressive strength of different mixes was found to depend on the coal bottom ash content; at 28 days of curing, mortars containing 10, 20, 30, 50, 70, 80 and 100 % coal bottom ash demonstrated compressive strength of 99.04, 93.98, 88.11, 82.14, 79.74, 77.61 and 67.97 %, respectively, when compared to that of the control mortar (Table 7), thus showing a slight decrease in strength with increasing coal bottom ash content. Nevertheless, as can be seen, the replacement of sand with coal bottom ash up to 50 % in content did not strongly affect compressive strength since the strength of the 50 % coal bottom ash mortar at 3, 7, 14, 28 and 60 days decreased by only 13.49, 15.79, 12.27, 17.86 and 19.68 %, respectively (Table 7). This decrease in compressive strength can be ascribed to two factors: the increase in porosity in mortars and the replacement of dense aggregate with porous aggregate (Fig. 2). Compressive strength is related to microstructure as shown earlier, where free water available for absorption through the porous coal bottom ash particles may contribute to pore formation and possibly lead to the decrease in strength.

Further, it seems that coal bottom ash has no significant negative effect on compressive strength since the

Table 5 Summary of the result and relative thermal conductivity at 28 days in comparison to control mix

Mix	Thermal conductivity (W/m K)	Relative thermal conductivity (%)
M0BA	1.666	100 (Control mortar)
M10BA	1.616	97.00
M20BA	1.532	91.96
M30BA	1.376	82.59
M50BA	1.070	64.23
M70BA	0.924	55.46
M80BA	0.783	47.00
M100BA	0.523	31.39
C0BA	2.052	100 (Control concrete)
C20BA	1.801	87.75
C50BA	1.493	72.74
C80BA	1.296	63.17
C100BA	1.089	53.09

$Y = 3.4296 - 0.0787x$

$R^2 = 0.9854$
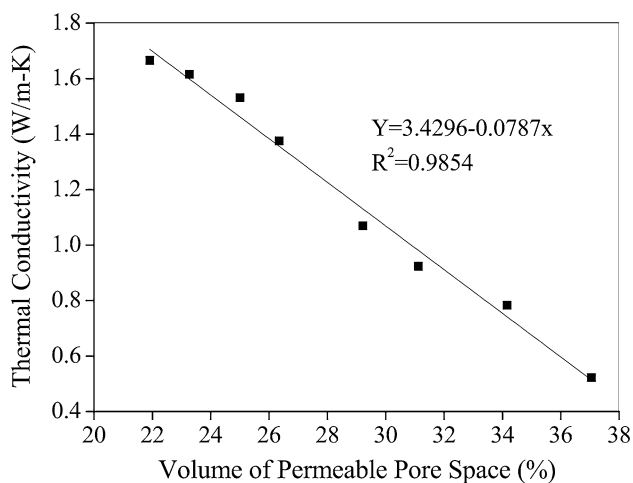
Fig. 6 Relationship between thermal conductivity and volume of permeable pore space

compressive strength of concrete containing 100 % coal bottom ash (31.39 MPa at 28 days) was very similar to that of the control (32.84 MPa at 28 days). This can be understood as resulting from the fact that the reduction in the proportion of fine to total aggregate with the use of coarse aggregate possibly results in lower effects on fine aggregates.

Microstructure

Given the fact that the mechanical properties of materials depend on their intrinsic microstructure [28], a comparison of the microstructure of mortars made with coal bottom ash and conventional mortar (the control mortar) is described in this section. The SEM image of the 50 % BA mortar shows a good mechanical interlocking connection between the rough surface of the coal bottom ash particle and

Fig. 7 Cross-section images of **a** mortar without coal bottom ash and **b** mortar with 100 % coal bottom ash

Table 6 Summary of compressive strength at various ages

Mix	Age					
	3 days (MPa)	7 days (MPa)	14 days (MPa)	28 days (MPa)	60 days (MPa)	160 days (MPa)
M0BA	33.74	36.85	40.44	49.21	58.04	–
M10BA	31.82	35.32	38.93	48.74	54.18	–
M20BA	31.49	33.51	38.19	46.25	50.52	–
M30BA	30.95	32.24	36.28	43.36	47.79	–
M50BA	29.19	31.03	35.48	40.42	46.62	–
M70BA	27.95	30.24	33.19	39.24	45.79	–
M80BA	25.16	30.18	32.51	38.19	44.62	–
M100BA	22.59	27.20	30.28	33.45	38.70	–
C0BA	–	21.92	–	32.84	–	40.80
C20BA	–	20.77	–	32.26	–	39.82
C50BA	–	20.67	–	31.55	–	39.05
C80BA	–	20.59	–	31.41	–	38.73
C100BA	–	20.50	–	31.39	–	37.97

Table 7 Relative compressive strength at various ages in comparison to the control mix

Mix	Age					
	3 days (%)	7 days (%)	14 days (%)	28 days (%)	60 days (%)	160 days (%)
M0BA	100 (Control mortar)					
M10BA	94.31	95.85	96.27	99.04	93.35	–
M20BA	93.33	90.94	94.44	93.98	87.04	–
M30BA	91.73	84.49	89.71	88.11	82.34	–
M50BA	86.51	84.21	87.73	82.14	80.32	–
M70BA	82.84	82.06	82.07	79.74	78.89	–
M80BA	74.57	81.90	80.39	77.61	76.88	–
M100BA	66.95	73.81	74.88	67.97	66.68	–
C0BA	100 (Control concrete)					
C20BA	–	94.75	–	98.23	–	97.60
C50BA	–	94.30	–	96.07	–	95.71
C80BA	–	93.93	–	95.65	–	94.93
C100BA	–	93.52	–	95.58	–	93.06

cement paste since small cracks could clearly be seen between the cement paste and the sand particles (showing a smooth surface), whereas no significant cracks were found between coal bottom ash particles and cement paste (Fig. 9). This may be due to the rougher surface of the coal bottom ash which improved the grip between the paste and the aggregate [12]. Therefore, it would seem that this should lead to an increase in compressive strength [12]; however, this investigation found that the compressive strength of the mortar decreased with an increase in coal bottom ash content. This can be explained by the voids in the mortar which were generated from excess water absorbed by the ash, and these may have more effect on compressive strength than the solid bond developed at the interfacial zone between the cement paste and the coal bottom ash aggregate.

In addition, SEM analyses of the mortar fragments composed of varying proportions of coal bottom ash are shown in Fig. 10. As can be seen from this, the control mortar was denser than the mortars containing bottom ash. In particular, tiny pores were found in the coal bottom ash mortar structure (0.1–10.0 μm in size) and it seems that the replacement of sand with coal bottom ash leads to pore formation in the structure. This finding supports the results of investigating the effects of bottom ash on permeability and compressive strength as reported earlier, since the number of pores noticeably increased with the use of coal bottom ash.
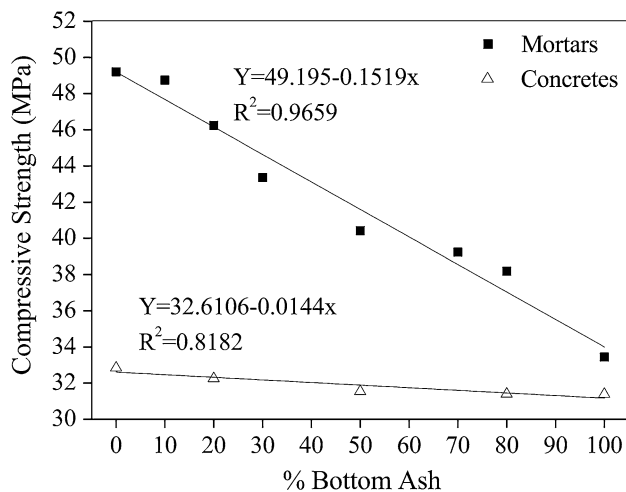
Fig. 8 Relationship between compressive strength and amount of coal bottom ash in mortars and concretes at the age of 28 days
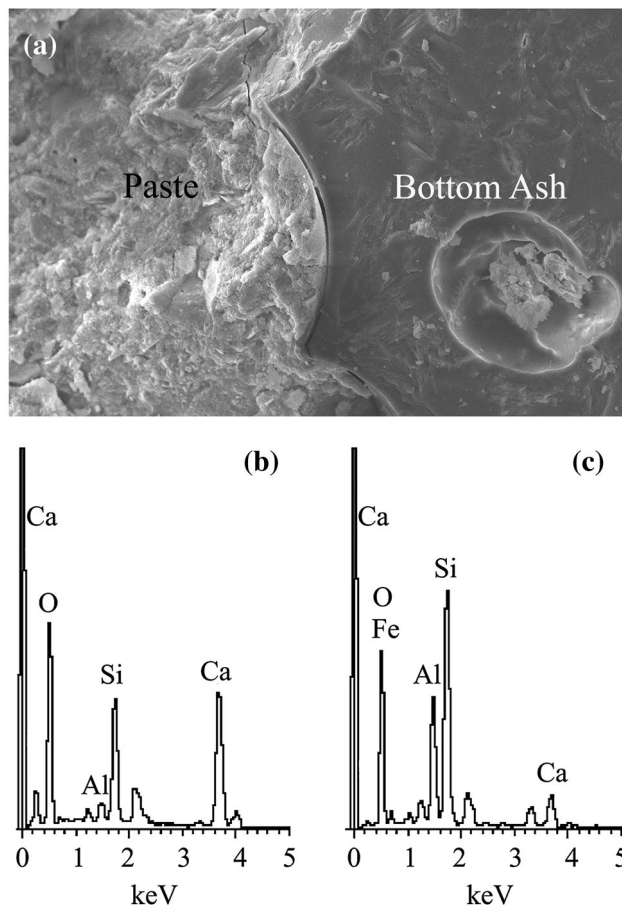

Fig. 9 Microstructure of mortars containing coal bottom ash. **a** SEM micrograph, **b** EDS spectrum of paste and **c** EDS spectrum of bottom ash

XRD analysis

Investigation of the various phases occurring in the hardened mortars with and without coal bottom ash was carried out using X-ray diffraction. After 28 days of curing, small pieces were removed from the middle of the hardened mortar and immersed in acetone for 48 h to stop the hydration reaction. These were then dried in a desiccator at 40 °C. The dried specimens were ground and sieved through a 90-μm sieve. The XRD tests were performed for diffraction angle (2θ) ranges of 5–80° in steps of 2θ = 0.012. The X-ray pattern of mortars containing 0, 20, 50, 80 and 100 % coal bottom ash are presented in Fig. 11. In all mortars, calcium silicate hydrate and unhydrated phases, such as dicalcium silicate and tricalcium silicate, were not clearly seen, implying that they tend to be swamped by the strong crystalline peak of Portlandite and Quartz. In addition, the intensity peak of Quartz was found to correlate with the use of coal bottom ash in mortars since the intensity peak of Quartz was predominant in mortar with a higher amount of sand.

Conclusions

This research presents the effects of coal bottom ash on the microstructure and mechanical properties of mortars and concretes. Experiments were conducted by replacing natural sand with coal bottom ash in varying percentages in mortars and concretes. Based on the analysis of the test results, the following conclusions can be drawn:

1. The density of mortars and concretes was noticeably decreased with increasing coal bottom ash. This is due to the lower specific gravity of coal bottom ash and the increase in pore volume.
2. The quantity of permeable pore space and the water absorption of mortars and concretes at 28 days were consistent with the results of the density tests. Levels of these were found to increase with increased levels of coal bottom ash. The permeable pore space of mortars and concretes increased from 21.91 to 37.05 % and 15.48 to 21.31 %, respectively, with the use of 100 % coal bottom ash when compared to that of the control mix.
3. With regard to the thermal conductivity test, it is interesting to note that the use of coal bottom ash as fine aggregate replacement improved thermal insulation since thermal conductivity showed a significant and linear decrease with increasing coal bottom ash
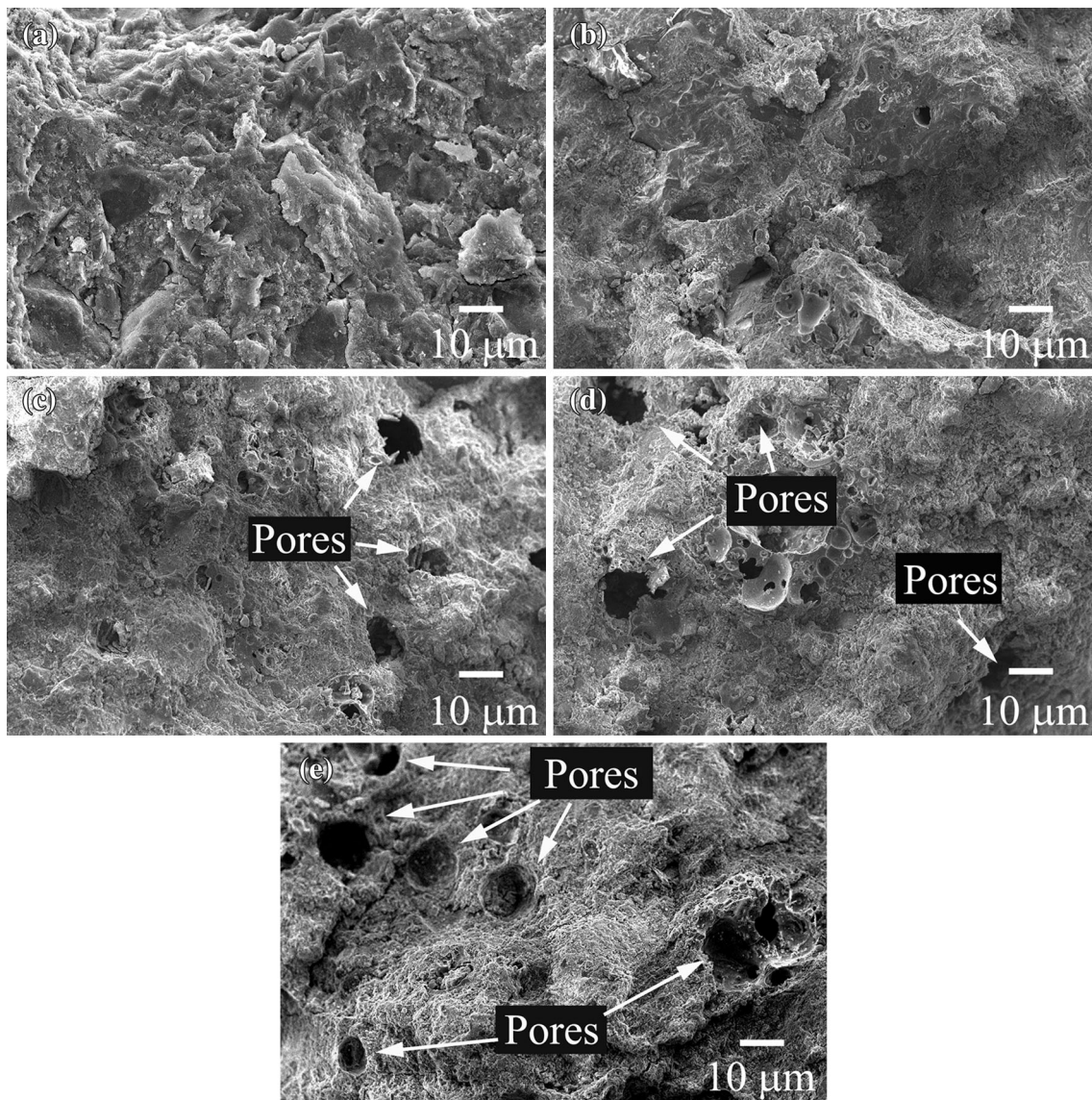
Fig. 10 SEM micrographs show the tiny pores in mortars structure containing **a** 0 %, **b** 20 %, **c** 50 %, **d** 80 % and **e** 100 % coal bottom ash

content. This is probably due to the porous structure of coal bottom ash and the high volume of permeable pore space in the test specimens since the thermal conductivity of mortar and concrete made with 100 % coal bottom ash was reduced by 68.61 and 46.91 %, respectively, as compared to that of the control mix. Moreover, although the permeable pore space of mortars and concretes increased with increasing coal bottom ash content, there is no detrimental effect on compressive strength for mortars and concretes since all mortars and concretes gained compressive strength approximately or more than 30 MPa at the age of 28 days. Therefore, these have the potential to be developed as an energy-saving building material such as heat-insulation blocks or precast concrete walls in the future.

4. The replacement of fine aggregate with coal bottom ash did not negatively affect the compressive strength of the concrete, as the compressive strength of concrete containing 100 % coal bottom ash (31.39 MPa at 28 days) was very similar to that of the control (32.84 MPa at 28 days). As well as in mortar, the replacement of sand with coal bottom ash at up to 50 % by volume did not strongly affect compressive strength; the strength of the 50 % coal bottom ash mortar at 28 days decreased by only 17.86 %.

5. The SEM tests were in agreement with the data on permeable pore space since the number of pores noticeably increased with the amount of coal bottom ash. The average pore sizes were between 0.1 and 10.0 µm.
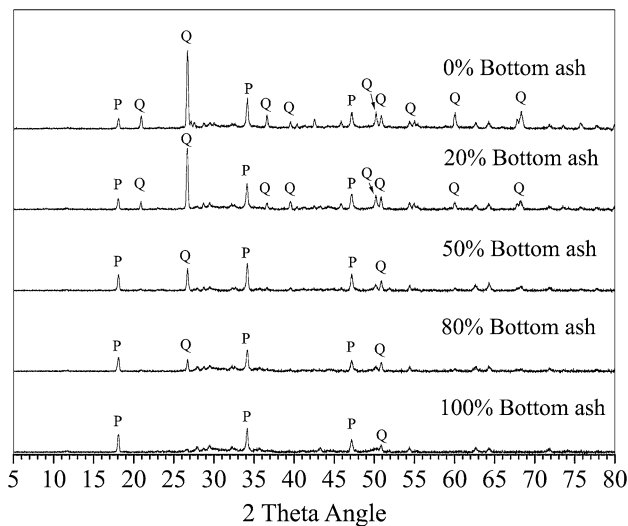
Fig. 11 X-ray diffraction pattern of mortars containing various amounts of coal bottom ash at 28 days, where *P* calcium hydroxide and *Q* quartz

References

1. Murari K, Siddique R, Jain KK (2015) Use of waste copper slag, a sustainable material. J Mater Cycles Waste Manag 17:13–26. doi:10.1007/s10163-014-0254-x

2. Ural N, Karakurt C, Cümert AT (2014) Influence of marble wastes on soil improvement and concrete production. J Mater Cycles Waste Manag 16:500–508. doi:10.1007/s10163-013-0200-3

3. Nayef AM, Fahad AR, Ahmed B (2010) Effect of microsilica addition on compressive strength of rubberized concrete at elevated temperatures. J Mater Cycles Waste Manag 12:41–49. doi:10.1007/s10163-009-0243-7

4. Nisnevich M, Sirotin G, Schlesinger T, Eshel Y (2008) Radiological safety aspects of utilizing coal ashes for production of lightweight concrete. Fuel 87:1610–1616. doi:10.1016/j.fuel.2007.07.031

5. Hinojosa MJR, Galvin AP, Agrela F, Perianes M, Barbudo A (2014) Potential use of biomass bottom ash as alternative construction material: conflictive chemical parameters according to technical regulations. Fuel 128:248–259. doi:10.1016/j.fuel.2014.03.017

6. Malhotra VM, Mehta PK (1996) Pozzolanic and cementitious materials. Advances in concrete technology, vol 1. Gordon & Breach Publishers, New York

7. Alonso JL, Wesche K (1991) Characterization of fly ash. In: Wesche K (ed) Fly ash in concrete. E & FN SPON, London

8. Siddique R, Khatib JM (2010) Abrasion resistance and mechanical properties of high-volume fly ash concrete. Mater Struct 43:709–718. doi:10.1617/s11527-009-9523-x

9. Zuquan J, Wei S, Yunsheng Z, Jinyang J, Jianzhong L (2007) Interaction between sulfate and chloride solution attack of concretes with and without fly ash. Cem Concr Res 37:1223–1232. doi:10.1016/j.cemconres.2007.02.016

10. Khaliq W, Kodur V (2013) Behavior of high strength fly ash concrete columns under fire conditions. Mater Struct 46:857–867. doi:10.1617/s11527-012-9938-7

11. Torgal FP, Jalali S (2011) Compressive strength and durability properties of ceramic wastes based concrete. Mater Struct 44:155–167. doi:10.1617/s11527-010-9616-6

12. Torkittikul P, Chaipanich A (2010) Utilization of ceramic waste as fine aggregate within Portland cement and fly ash concretes. Cem Concr Comp 32:440–449. doi:10.1016/j.cemconcomp.2010.02.004

13. Siddique R, Khatib JB, Kaur I (2008) Use of recycled plastic in concrete: a review. Waste Manage 28:1835–1852. doi:10.1016/j.wasman.2007.09.011

14. Konin A (2011) Use of plastic wastes as a binding material in the manufacture of tiles: case of wastes with a basis of polypropylene. Mater Struct 44:1381–1387. doi:10.1617/s11527-011-9704-2

15. Penacho P, Brito J, Veiga MR (2014) Physico-mechanical and performance characterization of mortars incorporating fine glass waste aggregate. Cem Concr Compos 50:47–59. doi:10.1016/j.cemconcomp.2014.02.007

16. Sharifi Y, Houshiar M, Aghebati B (2013) Recycled glass replacement as fine aggregate in self-compacting concrete. Front Struct Civ Eng 7(4):419–428. doi:10.1007/s11709-013-0224-8

17. Saikia N, Brito J (2014) Mechanical properties and abrasion behaviour of concrete containing shredded PET bottle waste as a partial substitution of natural aggregate. Con Build Mater 52:236–244. doi:10.1016/j.conbuildmat.2013.11.049

18. Singh M, Siddique R (2013) Effect of coal bottom ash as partial replacement of sand on properties of concrete. Resour Conserv Recycl 72:20–32. doi:10.1016/j.resconrec.2012.12.006

19. Ismail I, Bernal SA, Provis JL, Nicola RS, Brice DG, Kilcullen AR, Hamdan S, Deventer JSJ (2013) Influence of fly ash on the water and chloride permeability of alkali-activated slag mortars and concretes. Con Build Mater 48:1187–1201. doi:10.1016/j.conbuildmat.2013.07.106

20. Nath P, Sarker PK (2013) Effect of mixture proportions on the drying shrinkage and permeation properties of high strength concrete containing class F fly ash. KSCE J Civ Eng 17(6):1437–1445. doi:10.1007/s12205-013-0487-6

21. Wongkeo W, Thongsanitgarn P, Pimraksa K, Chaipanich A (2012) Compressive strength, flexural strength and thermal conductivity of autoclaved concrete block made using bottom ash as cement replacement materials. Mater Des 35:434–439. doi:10.1016/j.matdes.2011.08.046

22. Andrade LB, Rocha JC, Cheriaf M (2007) Evaluation of concrete incorporating bottom ash as a natural aggregates replacement. Waste Manage 27:1190–1199. doi:10.1016/j.wasman.2006.07.020

23. Lee HK, Kim HK, Hwang EA (2010) Utilization of power plant bottom ash as aggregates in fiber-reinforced cellular concrete. Waste Manage 30:274–284. doi:10.1016/j.wasman.2009.09.043

24. Yüksel İ, Bilir T, Özkan Ö (2007) Durability of concrete incorporating non-ground blast furnace slag and bottom ash as fine aggregate. Build Environ 42:2651–2659. doi:10.1016/j.buildenv.2006.07.003

25. Hussain K, Choktaweekarn P, Saengsoy W, Srichan T, Tangtermsirikul S (2013) Effect of cement types, mineral admixtures, and bottom ash on the curing sensitivity of concrete. Int J Min Met Mater 20:94–105. doi:10.1007/s12613-013-0699-2

26. Jayaranjan MLD, Hullebusch ED, Annachhatre AP (2014) Reuse options for coal fired power plant bottom ash and fly ash. Rev

Environ Sci Biotechnol 13:467–486. doi:10.1007/s11157-014-9336-4

27. Cheng A (2012) Effect of incinerator bottom ash properties on mechanical and pore size of blended cement mortars. Mater Des 36:859–864. doi:10.1016/j.matdes.2011.05.003

28. Singh M, Siddique R (2014) Strength properties and microstructural properties of concrete containing coal bottom ash as partial replacement of fine aggregate. Con Build Mater 50:246–256. doi:10.1016/j.conbuildmat.2013.09.026

29. Kim HK, Jeon JH, Lee HK (2012) Workability, and mechanical, acoustic and thermal properties of lightweight aggregate concrete with a high volume of entrained air. Con Build Mater 29:193–200. doi:10.1016/j.conbuildmat.2011.08.067

30. Wang KS, Chiou IJ, Chen CH, Wang D (2005) Lightweight properties and pore structure of foamed material made from sewage sludge ash. Con Build Mater 19:627–633. doi:10.1016/j.conbuildmat.2005.01.002

31. ASTM C150–12 (2012) Standard specification for Portland cement. American society for testing and materials

32. ASTM C33–13 (2013) Standard specification for concrete aggregates. American society for testing and materials

33. ASTM C127–12 (2012) Standard test method for density, relative density (specific gravity), and absorption of coarse aggregate. American society for testing and materials

34. ASTM C128–12 (2012) Standard test method for density, relative density (specific gravity), and absorption of fine aggregate. American society for testing and materials

35. ASTM C1437–13 (2013) Standard test method for flow of hydraulic cement mortar. American society for testing and materials

36. ASTM C143/C143M–12 (2012) Standard test method for slump of hydraulic-cement concrete. American society for testing and materials

37. ASTM C305–13 (2013) Standard practice for mechanical mixing of hydraulic cement pastes and mortars of plastic consistency. American society for testing and materials

38. ASTM C642–13 (2013) Standard test method for density, absorption, and voids in hardened concrete. American society for testing and materials

39. ASTM D5334–14 (2014) Standard test method for determination of thermal conductivity of soil and soft rock by thermal needle probe procedure. American society for testing and materials

40. ASTM C192/C192M–13a (2013) Standard practice for making and curing concrete test specimens in the laboratory. American society for testing and materials

41. Naganathan S, Razak H, Hamid SNA (2012) Properties of controlled low-strength material made using industrial waste incineration bottom ash and quarry dust. Mater Des 33:56–63. doi:10.1016/j.matdes.2011.07.014

42. Wu W, Zhang W, Ma G (2010) Optimum content of copper slag as a fine aggregate in high strength concrete. Mater Des 31:2878–2883. doi:10.1016/j.matdes.2009.12.037

43. Collins F, Sanjayan J (2009) Prediction of convective transport within unsaturated concrete utilizing pore size distribution data. J Porous Mater 16:651–656. doi:10.1007/s10934-008-9245-4

44. Bernardo E, Scarinci G, Bertuzzi P, Ercole P, Ramon L (2010) Recycling of waste glasses into partially crystallized glass foams. J Porous Mater 17:359–365. doi:10.1007/s10934-009-9286-3